Optical pumping magnetic resonance in high magnetic fields: Characterization of nuclear relaxation during pumping

Matthew P. Augustine and Kurt W. Zilm
Department of Chemistry, Yale University, New Haven, Connecticut 06511

(Received 21 April 1995; accepted 16 February 1996)

The polarization of ^{129}Xe gas by spin exchange with optically pumped Rb vapor is investigated in high magnetic field. Operation in a high field provides added spectral dispersion via Zeeman shifts of the electronic transitions. This simplifies the physics of the pumping process in such a way as to make it more amenable to treatment with simple rate theory. A relationship between the steady state ^{129}Xe polarization and the applied laser power is derived which agrees with experimental results. This theory serves as a guide to the manufacture of very high polarizations of ^{129}Xe gas. © *1996 American Institute of Physics.* [S0021-9606(96)02519-X]

I. INTRODUCTION

Optical pumping has been researched extensively in the past few decades following the pioneering work of Kastler in the 1950's.[1] Recently there has been an increased amount of study involving the indirect pumping of nuclear spins via spin exchange with optically polarized valence electrons of another atom.[2] The magnetic resonance signal for nuclei polarized in this fashion is greatly enhanced in comparison to that achieved with the typically small Boltzmann equilibrium polarization. In all of the research efforts to date however, the optical pumping phenomena has not been thoroughly examined in multi-tesla magnetic fields. In this paper we describe optical pumping of ^{129}Xe via spin exchange at fields up to 7.04 T. By polarizing at high fields we show that ^{129}Xe nuclear spin polarization can be more efficiently produced in comparison to lower fields. This is largely due to elimination of photon depolarization mechanisms and better suppression of wall relaxation. Furthermore, the kinetics of the polarization exchange are simpler to model theoretically in the high field case. The advantage of using Zeeman shifts to resolve the optical transitions involved in the optical pumping process is also demonstrated.

Previous treatments of the optical orientation of alkali atoms have typically been cast in terms of time dependent perturbation theory.[3] In the following we provide an equivalent alternate description for optical pumping in high field using the formalism of spin lattice relaxation. This approach is useful in that it naturally leads to equations for the spin exchange polarization of ^{129}Xe that parallel those used commonly to describe the well known nuclear Overhauser effect.[4] In this manner we obtain expressions that relate the ^{129}Xe polarization to the available incident laser power. Nuclear magnetic resonance (NMR) spectroscopists interested in chemical applications[2] of spin polarized ^{129}Xe will find this more familiar theoretical framework useful in their design of experiments utilizing this potentially powerful source of high spin polarization. These results are tested experimentally and discussed in terms so that one can objectively judge the efficiency of an optical pumping apparatus for generating high polarizations of ^{129}Xe.

II. THEORY

Placement of Rb into a high magnetic field uncouples its nuclear spin angular momentum I from J, the resultant of coupling the electron orbital angular momentum L, and the electron spin angular momentum S, as $J=L+S$. The transition to these states at higher magnetic fields from the usual $|F,m_F\rangle$ levels in low field is shown in Fig. 1 for ^{85}Rb ($I=5/2$). If the magnetic field is high enough, the ^{85}Rb electronic energy levels are best described as product states, $|m_J,m_I\rangle$, labeled with coupled orbital and electron spin, m_J, and nuclear spin, m_I, quantum numbers. These states group together into a band of energy levels with common values of L and m_J and all possible values of m_I in high field as shown in Fig. 1. This band of states is centered in energy about the appropriate field split Russell–Saunders atomic term, $|L,m_J\rangle$, that would result if nuclear hyperfine effects were neglected.[5] This is also the case for the lower natural abundance isotope, ^{87}Rb, even though there is a slightly larger hyperfine coupling to its $I=3/2$ nuclear spin.[6] Since electronic transitions conserve m_I, the optical pumping dynamics with ^{85}Rb can be considered separately for each manifold of four such states having the same m_I. As long as the nuclear hyperfine coupling is negligible compared to the bandwidth of the applied laser light, a simplified energy level diagram using the field split Russell–Saunders atomic terms alone suffices for our purposes. In what follows we consider optical pumping between the levels described by these magnetic field split Russell–Saunders atomic terms as shown in Fig. 2.

For Rb, the ground and first excited state atomic terms are $^2S_{1/2}$ and $^2P_{1/2}$ corresponding to [Kr] $5s^1$ and [Kr] $5p^1$ electron configurations, respectively. As just discussed, these atomic terms are further split by B_0 into two $m_J=\pm 1/2$ levels, $|S,\pm\rangle$ and $|P,\pm\rangle$, as shown in Fig. 2, where the kets are now labeled by just the orbital quantum number (S or P) and the z projection of the coupled electron orbital and spin angular momenta ($\pm$). Irradiation of this system with σ_+ laser light will move population from $|S,-\rangle$ to $|P,+\rangle$ at a rate R. This excited state population subsequently fluoresces back to the ground state by emission of either a σ_+ or π polarized photon. The probability of emitting a σ_+ photon is scaled by

 0021-9606/96/105(8)/2998/14/$10.00

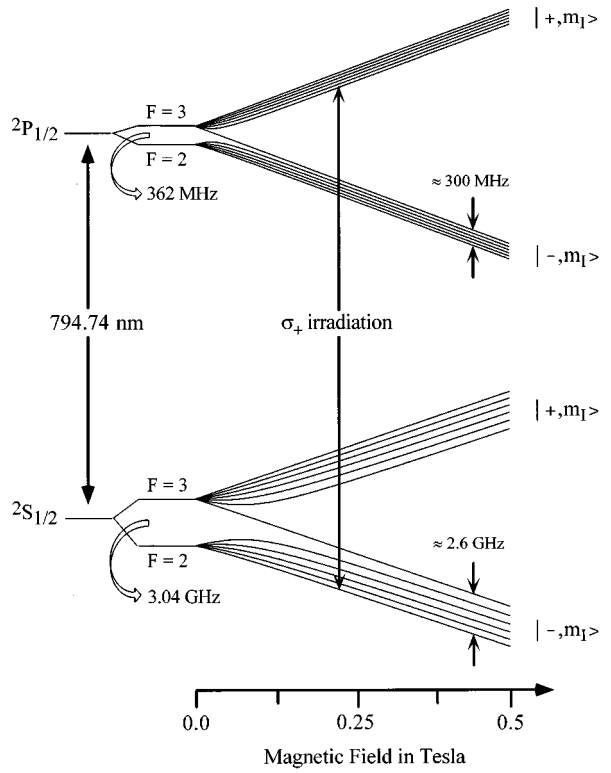

FIG. 1. Energy level diagram showing the ground and first excited states of ^{85}Rb including the effects of hyperfine coupling as a function of B_0. Notice that as the field increases, m_F is no longer a good quantum number and the levels group together with common electron spin value.

2/3 while that for a π photon is scaled by 1/3. This unequal weighting of the total emission rate shown in Fig. 2 comes directly from the angular momentum selection rules for the $|P,+\rangle \rightarrow |S,\pm\rangle$ transitions. The spins deposited in $|S,-\rangle$ are recycled by the laser to $|P,+\rangle$ while population builds up in $|S,+\rangle$, thus producing a net orientation of the Rb electron

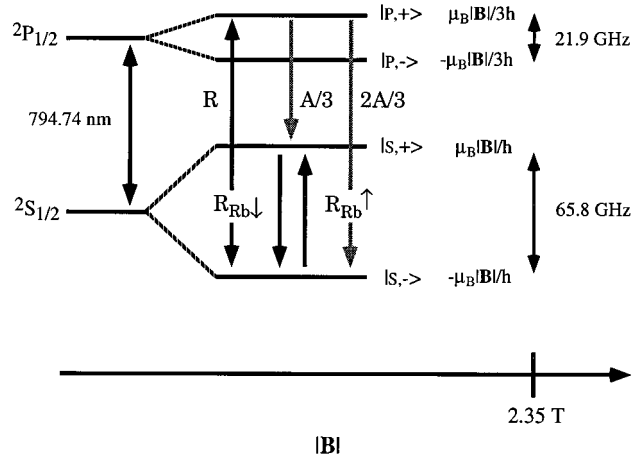

FIG. 2. Ground state and first excited state of Rb in high magnetic field and during optical pumping. The pump rate, R, fluorescence lifetime, $1/A$, and ground state spin lattice relaxation and spin exchange rates, $R_{\mathrm{Rb}}\downarrow$ and $R_{\mathrm{Rb}}\uparrow$, all effect the ground state sublevel populations.

magnetic moment in the ground state. One should be clear that the optical transition does not in itself effect a flip of the Rb electron spin. In the ground S state the electron spin m_S is quantized in the frame defined by the applied field, i.e., m_S is a good quantum number. However, in the excited P state the large spin orbit coupling mixes the $m_S = \pm 1/2$ states. Transitions to this state then make it possible for the system to decay back to the $|S,+\rangle$ state even though a magnetic dipole transition operator is not directly involved.

If it were not for the ground state electron spin lattice relaxation, all of the population would eventually end up in $|S,+\rangle$. Therefore, in order to produce a high Rb electron spin polarization, the buildup of polarization via optical pumping must be fast compared to the leakage due to spin lattice relaxation. As the following treatment will make clear, obtaining high ^{129}Xe spin polarization requires production of a high Rb electron spin polarization. Thus a natural starting point is the dynamics of the optical polarization of the Rb.

A. Optical polarization of Rb in the presence of ^{129}Xe

In a sample containing only Rb atoms and a spinless buffer gas, the electron spin lattice relaxation rate can be quite long, and is principally due to fluctuating fields caused by Rb–Rb collisions or by collisions with the cell walls or the buffer gas. The rates for flipping the Rb electron spin down or up that result from these fluctuations will be denoted $W_{\mathrm{Rb}}\downarrow$ and $W_{\mathrm{Rb}}\uparrow$, respectively. The Rb electron spin lattice relaxation time constant, T_1^{Rb}, is related to these rates in the usual fashion,

$$\frac{1}{T_1^{\mathrm{Rb}}} = W_{\mathrm{Rb}}\downarrow + W_{\mathrm{Rb}}\uparrow. \tag{1}$$

When the buffer gas has a nuclear spin, as in the case of ^{129}Xe, this inherent relaxation is augmented by Rb–^{129}Xe cross relaxation. As described elsewhere, this is due to the fluctuating hyperfine field the Rb electrons experience from interacting with the ^{129}Xe nuclei.[7] This additional component to the Rb electron relaxation is proportional to the number density of the ^{129}Xe, N_{Xe}, and what has been called the velocity averaged spin exchange cross section, $\langle \sigma \overline{v} \rangle$.[7] The net Rb spin lattice relaxation rate is then characterized by the time constant $T_1^{\mathrm{Rb}*}$,

$$\frac{1}{T_1^{\mathrm{Rb}*}} = \frac{1}{T_1^{\mathrm{Rb}}} + N_{\mathrm{Xe}} \langle \sigma \overline{v} \rangle. \tag{2}$$

In describing the dynamics of the optical orientation of the Rb in the presence of ^{129}Xe, it is useful to define net transition probabilities for flipping the Rb electron spin which take into account the cross relaxation term. As stated earlier, the cross relaxation is mediated by the hyperfine interaction of the Rb electron (**S**) with a ^{129}Xe nucleus (**I**). Since this Hamiltonian is of the form $\mathscr{A}\mathbf{I}\cdot\mathbf{S} = \mathscr{A}[I_z S_z + 1/2(I_+ S_- + I_- S_+)]$,[7] only mutual Rb electron–^{129}Xe nucleus spin flip transitions are involved. The net Rb electron spin flip rates then depend upon the ^{129}Xe nuclear spin state specific number densities, N_{Xe}^- or N_{Xe}^+. The

cross relaxation contributes $N_{\mathrm{Xe}}^{-}\langle\sigma\overline{v}\rangle$ to the down rate, and $N_{\mathrm{Xe}}^{+}\langle\sigma\overline{v}\rangle$ to the up rate. Combining the cross relaxation and other spin lattice contributions gives the net Rb electron transition rates, $R_{\mathrm{Rb}}\uparrow$ and $R_{\mathrm{Rb}}\downarrow$, as

$$R_{\mathrm{Rb}}\downarrow = W_{\mathrm{Rb}}\downarrow + N_{\mathrm{Xe}}^{-}\langle\sigma\overline{v}\rangle,$$
$$R_{\mathrm{Rb}}\uparrow = W_{\mathrm{Rb}}\uparrow + N_{\mathrm{Xe}}^{+}\langle\sigma\overline{v}\rangle. \tag{3}$$

The three level system shown in Fig. 2 provides a convenient framework for modeling the optical polarization of the Rb. In a typical experimental setup, where the light is of just one polarization, the effect of the pumping light over most of the sample cell is to introduce a laser intensity dependent rate process with rate R that connects the pair of states in the optical transition. This simplification makes it possible to describe the pumping dynamics with a set of coupled differential equations for the level populations using rate theory. Our goal is to calculate the polarization of the Rb electron, P_{Rb}, which is defined here as the total number of spins per unit volume down, $N_{\mathrm{Rb}}^{-}=N_S^{-}$, minus the total number of spins per unit volume up, $N_{\mathrm{Rb}}^{+}=N_S^{+}+N_P^{+}$, divided by the total Rb number density, N_{Rb}. Notice that the contribution of the level $|P,-\rangle$ has been ignored as there are no significant relaxation pathways connecting it to any of the other energy levels. Photons of other polarizations will connect $|P,-\rangle$ to the rest of the system. Including these effects at this point would just confuse the basic physics, and we will return to these complications later. Using these definitions, the appropriate rate equations in this case are

$$\frac{dN_S^{-}}{dt} = -(R+R_{\mathrm{Rb}}\uparrow)N_S^{-} + \left(R+\frac{2}{3}A\right)N_P^{+} + R_{\mathrm{Rb}}\downarrow N_S^{+},$$
$$\frac{dN_S^{+}}{dt} = -R_{\mathrm{Rb}}\downarrow N_S^{+} + R_{\mathrm{Rb}}\uparrow N_S^{-} + \frac{1}{3}AN_P^{+},$$
$$\frac{dN_P^{+}}{dt} = -(R+A)N_P^{+} + RN_S^{-}. \tag{4}$$

As written, these equations implicitly involve the polarization of the ^{129}Xe spin states through the cross relaxation terms included in $R_{\mathrm{Rb}}\uparrow$ and $R_{\mathrm{Rb}}\downarrow$. In principal then, a complete solution of Eqs. (4) would also include consideration of another set of coupled equations involving the ^{129}Xe spin level populations. However, if we are only interested in the steady state value of P_{Rb}, the steady state values for N_{Xe}^{-} or N_{Xe}^{+} can be used. With this approximation the steady state value of P_{Rb} can be shown to be given by

$$P_{\mathrm{Rb}} = \frac{N_S^{-}-N_S^{+}-N_P^{+}}{N_{\mathrm{Rb}}} = \frac{1-\beta}{1+\beta}, \tag{5}$$

where

$$\beta = \frac{R}{R+A}\left(1+\frac{A}{3R_{\mathrm{Rb}}\downarrow}\right) + \frac{R_{\mathrm{Rb}}\uparrow}{R_{\mathrm{Rb}}\downarrow} \tag{6}$$

and all level populations are understood to be those found under steady state conditions.

It is useful to examine P_{Rb} in various limits in order to gain some physical insight into the dynamics of optical pumping. In the most commonly encountered experimental situation, the fastest rate process will be spontaneous emission from the upper electronic state. Taking A as essentially infinite in this case, the polarization can be written as

$$P_{\mathrm{Rb}} = \frac{R_{\mathrm{Rb}}\downarrow - R_{\mathrm{Rb}}\uparrow - \frac{R}{3}}{R_{\mathrm{Rb}}\downarrow + R_{\mathrm{Rb}}\uparrow + \frac{R}{3}}. \tag{7}$$

This result also directly follows from Eqs. (4) if the rate term AN_p^{+} is replaced by RN_s^{-} in each instance. When a spinless buffer gas is considered, $R_{\mathrm{Rb}}\downarrow$ and $R_{\mathrm{Rb}}\uparrow$ reduce to $W_{\mathrm{Rb}}\downarrow$ and $W_{\mathrm{Rb}}\uparrow$. Equation (7) can then be written in terms of the Boltzmann Rb polarization, P_{Rb}^{0}, T_1^{Rb}, and the pump rate R. P_{Rb} in this limit is

$$P_{\mathrm{Rb}} = \frac{P_{\mathrm{Rb}}^{0} - \frac{1}{3}RT_1^{\mathrm{Rb}}}{1+\frac{1}{3}RT_1^{\mathrm{Rb}}}. \tag{8}$$

This equation illustrates the expected result; in the absence of irradiation ($R\rightarrow 0$), $P_{\mathrm{Rb}}=P_{\mathrm{Rb}}^{0}$, and in the limit of very efficient pumping ($R\rightarrow\infty$), $P_{\mathrm{Rb}}\rightarrow -1$. It also points out the fundamental requirement on the intensity of the pumping light; it must produce a pump rate R that can dominate the Rb ground state electron depolarization rate, $1/T_1^{\mathrm{Rb}}$, if one is to achieve a significant polarization.

B. Spin exchange between ^{129}Xe and optically pumped Rb

The spin exchange polarization of ^{129}Xe by optically pumped Rb can also be understood in a straightforward fashion using simple rate theory.[8] In a high magnetic field the ^{129}Xe relaxation is well described by a standard two level system where the two spin states are connected by two unequal spin flip rates, $R_{\mathrm{Xe}}\downarrow$ and $R_{\mathrm{Xe}}\uparrow$. These rates have contributions from high field spin lattice relaxation in the absence of the Rb, $W_{\mathrm{Xe}}\downarrow$, and $W_{\mathrm{Xe}}\uparrow$, in addition to the spin exchange relaxation with the Rb electron. As discussed earlier, the spin exchange is governed by a Hamiltonian of the form $\mathscr{H}=\mathbf{I}\cdot\mathbf{S}$.[7] Only the flip–flop terms, $I_+S_-+I_-S_+$, can effect a mutual population change between the spin states of the Rb electron and the ^{129}Xe nuclei. Therefore, the net rate at which the ^{129}Xe$|+\rangle$ state spin flips to the $|-\rangle$ state depends on the number density of the Rb electron in the $|-\rangle$ state. In other words, the net up and down transition rates for the ^{129}Xe will be proportional to the number density of the Rb electron in a given spin orientation in direct analogy to Eq. (3).

However, upon closer consideration Eq. (3) can be shown to be incomplete. At thermal equilibrium the populations of both the Rb electron and the ^{129}Xe spins must approach Boltzmann in the absence of optical pumping. This requires the cross relaxation rates to be slightly different. Taking this additional complication into account we write

$$R_{\mathrm{Xe}}\downarrow = W_{\mathrm{Xe}}\downarrow + N^{-}_{\mathrm{Rb}}\langle\sigma\overline{v\uparrow}\rangle,$$

$$R_{\mathrm{Xe}}\uparrow = W_{\mathrm{Xe}}\uparrow + N^{+}_{\mathrm{Rb}}\langle\sigma\overline{v\downarrow}\rangle. \tag{9}$$

In Eqs. (9) the small difference in the two cross-relaxation rates as required by detailed balance have been included by differentiating them as $\langle\sigma\overline{v\downarrow}\rangle$ and $\langle\sigma\overline{v\uparrow}\rangle$. The direction of the arrow signifies whether the Rb electron transition is in either the upward or downward direction.

As shown in the previous section, the laser pump rate R only needs to beat the Rb electron relaxation to produce a significant electron polarization, and therefore a significant ^{129}Xe polarization. In most instances then the spontaneous emission rate A will be much greater than R. In this limit we can restrict our treatment to the S state populations for the Rb. Thus, the two equations in this effective ground state model for the Rb and ^{129}Xe spin populations that need be considered are

$$\begin{aligned}\frac{dN^{-}_{S}}{dt} &= -\frac{R}{3}N^{-}_{S} - W_{\mathrm{Rb}}\uparrow N^{-}_{S} + W_{\mathrm{Rb}}\downarrow N^{+}_{S} - N^{-}_{S}N^{+}_{\mathrm{Xe}}\langle\sigma\overline{v\uparrow}\rangle \\ &\quad + N^{+}_{S}N^{-}_{\mathrm{Xe}}\langle\sigma\overline{v\downarrow}\rangle, \\ \frac{dN^{-}_{\mathrm{Xe}}}{dt} &= -W_{\mathrm{Xe}}\uparrow N^{-}_{\mathrm{Xe}} + W_{\mathrm{Xe}}\downarrow N^{+}_{\mathrm{Xe}} - N^{-}_{\mathrm{Xe}}N^{+}_{S}\langle\sigma\overline{v\downarrow}\rangle \\ &\quad + N^{+}_{\mathrm{Xe}}N^{-}_{S}\langle\sigma\overline{v\uparrow}\rangle.\end{aligned} \tag{10}$$

These equations can be recast into more convenient forms involving the polarizations using $P_{\mathrm{Xe}}=(N^{-}_{\mathrm{Xe}}-N^{+}_{\mathrm{Xe}})/N_{\mathrm{Xe}}$, the Boltzmann equilibrium polarizations denoted as P^{0}_{Xe} and P^{0}_{Rb}, and the usual longitudinal relaxation times T_1,

$$\frac{1}{T^{\mathrm{Rb}}_1} = W_{\mathrm{Rb}}\uparrow + W_{\mathrm{Rb}}\downarrow,\quad \frac{1}{T^{\mathrm{Xe}}_1} = W_{\mathrm{Xe}}\uparrow + W_{\mathrm{Xe}}\downarrow,$$

$$P^{0}_{\mathrm{Rb}} = \frac{W_{\mathrm{Rb}}\downarrow - W_{\mathrm{Rb}}\uparrow}{W_{\mathrm{Rb}}\downarrow + W_{\mathrm{Rb}}\uparrow},\quad P^{0}_{\mathrm{Xe}} = \frac{W_{\mathrm{Xe}}\downarrow - W_{\mathrm{Xe}}\uparrow}{W_{\mathrm{Xe}}\downarrow + W_{\mathrm{Xe}}\uparrow}. \tag{11}$$

We also define a factor f and the spin exchange time T^{se}_1 in terms of the cross relaxation rates as follows:

$$f = \frac{\langle\sigma\overline{v\downarrow}\rangle - \langle\sigma\overline{v\uparrow}\rangle}{\langle\sigma\overline{v\downarrow}\rangle + \langle\sigma\overline{v\uparrow}\rangle},$$

$$\frac{1}{T^{\mathrm{se}}_1} = N_{\mathrm{Rb}}\frac{\langle\sigma\overline{v\downarrow}\rangle + \langle\sigma\overline{v\uparrow}\rangle}{2} = N_{\mathrm{Rb}}\langle\sigma\overline{v}\rangle. \tag{12}$$

With these definitions and using $\alpha=N_{\mathrm{Xe}}/N_{\mathrm{Rb}}$, Eqs. (10) can be recast as

$$\begin{aligned}\dot{P}_{\mathrm{Rb}} &= \frac{2}{N_{\mathrm{Rb}}}\frac{dN^{-}_{S}}{dt} = -\frac{R}{3}(1+P_{\mathrm{Rb}}) - \frac{(P_{\mathrm{Rb}}-P^{0}_{\mathrm{Rb}})}{T^{\mathrm{Rb}}_1} \\ &\quad + \frac{\alpha f}{T^{\mathrm{se}}_1}(1-P_{\mathrm{Rb}}P_{\mathrm{Xe}}) - \frac{\alpha}{T^{\mathrm{se}}_1}(P_{\mathrm{Rb}}-P_{\mathrm{Xe}}), \\ \dot{P}_{\mathrm{Xe}} &= \frac{2}{N_{\mathrm{Xe}}}\frac{dN^{-}_{\mathrm{Xe}}}{dt} = -\frac{(P_{\mathrm{Xe}}-P^{0}_{\mathrm{Xe}})}{T^{\mathrm{Xe}}_1} - \frac{f}{T^{\mathrm{se}}_1}(1-P_{\mathrm{Rb}}P_{\mathrm{Xe}}) \\ &\quad + \frac{1}{T^{\mathrm{se}}_1}(P_{\mathrm{Rb}}-P_{\mathrm{Xe}}).\end{aligned} \tag{13}$$

The ratio of the up and down spin exchange cross sections must be the Boltzmann factor for the mutual spin–flip transition, $\langle\sigma\overline{v\downarrow}\rangle/\langle\sigma\overline{v\uparrow}\rangle=\exp(+\Delta E/kT)$, where ΔE is the difference in the Rb electron and ^{129}Xe Zeeman splittings. From this fact, or by considering the second of Eqs. (13) at steady state, f can be shown to be

$$f = \frac{P^{0}_{\mathrm{Rb}} - P^{0}_{\mathrm{Xe}}}{1 - P^{0}_{\mathrm{Rb}}P^{0}_{\mathrm{Xe}}}. \tag{14}$$

The terms with f in Eqs. (13) are small, as f is only on the order of 10^{-3}, and they can usually be dropped. Their main purpose is to ensure that the proper Boltzmann equilibrium polarizations are achieved in the absence of any optical pumping.

Adding $\dot{P}_{\mathrm{Rb}}$ to $\alpha\dot{P}_{\mathrm{Xe}}$ in Eqs. (13) provides an equation independent of f, which when evaluated at steady state relates the steady state polarization of the Rb to that of the ^{129}Xe,

$$P_{\mathrm{Rb}} = \frac{P^{0}_{\mathrm{Rb}} - \frac{1}{3}RT^{\mathrm{Rb}}_1 - \alpha(P_{\mathrm{Xe}}-P^{0}_{\mathrm{Xe}})(T^{\mathrm{Rb}}_1/T^{\mathrm{Xe}}_1)}{1 + \frac{1}{3}RT^{\mathrm{Rb}}_1}. \tag{15}$$

This is to be compared to the expression arrived at earlier when the buffer gas was considered spinless [Eq. (8)]. To obtain an expression for the Rb polarization in terms of sample composition, relaxation times, and laser intensity alone, it is convenient to simplify the terms involving f. These terms which are quadratic in the polarizations also arise in cross relaxation problems at low temperature.[9] We will make use of the fact that the Boltzmann polarizations in our case are for high temperatures and therefore are quite small. As such we will set the term $f(1-P_{\mathrm{Rb}}P_{\mathrm{Xe}}) = (P^{0}_{\mathrm{Rb}}-P^{0}_{\mathrm{Xe}})(1-P_{\mathrm{Rb}}P_{\mathrm{Xe}})/(1-P^{0}_{\mathrm{Rb}}P^{0}_{\mathrm{Xe}})$ to $(P^{0}_{\mathrm{Rb}}-P^{0}_{\mathrm{Xe}})$. This still produces the proper limits in the absence of optical pumping, and avoids unphysical results that would occur if the term was simply dropped altogether. The error produced is the order of P^{0}_{Rb}. Within this approximation, the second of Eqs. (13) then provides the following simple result at steady state,

$$(P_{\mathrm{Xe}}-P^{0}_{\mathrm{Xe}}) = \gamma(P_{\mathrm{Rb}}-P^{0}_{\mathrm{Rb}}),$$

$$\text{where}\quad \gamma = \left\{\frac{1}{1+\frac{T^{\mathrm{se}}_1}{T^{\mathrm{Xe}}_1}}\right\}. \tag{16}$$

This equation states that the departure of the ^{129}Xe polarization from Boltzmann is the same as that for the Rb polarization due to the optical pumping within a multiplicative factor γ. The γ factor is a measure of how efficiently the ^{129}Xe nuclei are relaxed by the Rb as opposed to the wall relaxation, and γ is often close to 1. Since the ^{129}Xe and Rb polarizations are related by a constant factor, calculation of either one over the sample volume can be used to compare with experiment. We can now use this equation to substitute

for $(P_{Xe}-P^0_{Xe})$ in Eq. (15). This gives an expression for the Rb polarization in terms of the sample composition, pump rate, and inherent relaxation rates,

$$P_{Rb}=\frac{-1+\frac{3\epsilon}{R}P^0_{Rb}}{1+\frac{3\epsilon}{R}},\quad \text{where}\quad \epsilon=\left(\frac{1}{T_1^{Rb}}+\frac{\alpha\gamma}{T_1^{Xe}}\right). \tag{17}$$

Equation (17) states that the pump rate, R, needs to overcome a Rb relaxation rate, 3ϵ, which is a sum of the normal spin lattice relaxation of the Rb and leakage through the ^{129}Xe. Since α may easily be as large as 10^6, these two terms can in practice be quite comparable.

C. Finite thickness sample

In the thin sample limit where all of the photons are σ_+ polarized, the previous equation is all that is required to calculate P_{Xe} or P_{Rb} given the relaxation times and other experimental parameters. However, in most cases the sample to be polarized will not be optically thin and we must consider that the pump rate R, which depends upon the light intensity, will also depend upon the degree of spin polarization[10] and the location within the sample.

To proceed further we must adopt a model for the sample geometry and the pumping light. In the cases of interest to us, the sample will be cylindrical, with length l and radius r. The laser light beam will have a Gaussian profile in its frequency distribution and in its spatial profile. The intensity of the laser light then is given by a distribution function $\iota(\omega,r,z)$ which when integrated over frequency and the beam cross section gives the power $P_0(z)$ as a function of distance into the sample,

$$P_0(z)=2\pi\int_0^\infty\int_0^\infty \iota(\omega,r,z)r\,dr\,d\omega. \tag{18}$$

$P_0(0)=P_0$ will be taken as the power incident upon the plane at the beginning of the sample. The absorption of the light as the beam propagates through the sample is a first order process as a function of displacement in the sample. Power is removed from the beam in direct proportion to the number of absorbers, the rate at which they spontaneously emit and the energy of the photon involved,[11]

$$\frac{d\iota(\omega,r,z)}{dz}=-\frac{2}{3}\,\iota(\omega,r,z)N_A(z)g(\omega)\hbar\omega B_{12}/c. \tag{19}$$

In this equation $N_A(z)$ represents the number of absorbers at a position z. The function $g(\omega)$ is the atomic absorption line shape which gives the proportion of absorbers that are within $d\omega$ of the laser at the frequency ω, and B_{12} is the usual stimulated absorption coefficient. Again, the factor of 2/3 comes from the angular momentum selection rules for σ_+ light connecting $|S,-\rangle\rightarrow|P,+\rangle$. Notice that if π light were used different states, $|S,-\rangle\rightarrow|P,-\rangle$, would be connected in the Rb D_1 line and only a factor of 1/3 would be present in Eq. (19). In most experimental situations the laser intensity will be significantly greater than the fluorescence intensity, especially once the sample is significantly polarized. As such we are justified in neglecting any additional complications that might arise due to reabsorption of this small number of photons at other polarizations. This radiation trapping[12] only provides an additional relaxation mechanism for the ground state Rb polarization and can be adequately compensated for in the value of T_1^{Rb} as mentioned below.

In most instances the Rb atomic absorption line shape will be dominated by pressure broadening from collisions with the Xe buffer gas. In cells approaching 1 atm in pressure, this broadening will be the order of 80 GHz. Typical Ti:sapphire lasers, which are convenient light sources, have significantly narrower spectral profiles than this (2 GHz typical). Therefore, as far as the light profile is concerned, the atomic absorption is essentially a constant across the laser profile. In this case we can integrate out the frequency dependence and write for σ_+ light that

$$\frac{dI(r,z)}{dz}=-\frac{2}{3}\,\hbar\omega_0 B_{12}\Omega I(r,z)N_A(z)/c. \tag{20}$$

The term Ω is the integral of the laser profile over the atomic line shape,

$$\Omega=\int_0^\infty g(\omega)\iota(\omega)d\omega. \tag{21}$$

In order to separate out the frequency and spatial variation of the laser light we have used the fact that the atomic line shape is homogeneously broadened and much wider than the laser profile, both very good assumptions in the case under consideration. In this case, the frequency dependence of Ω gives the spectrum of the Rb D_1 line. Taking the line shape as a pressure broadened Lorentzian and assuming that the laser is on resonance, $\Omega=2/(\pi\Delta_{1/2})$, where $\Delta_{1/2}$ is the full-width at half-height of the atomic absorption in angular frequency units (rad/s). For convenience we define $\kappa=2B_{12}\Omega/3c$. The frequency averaged pump rate R is then given by $\kappa I(r,z)$.

Since the pump rate R depends upon $I(r,z)$, the polarization will also vary across the sample. To account for this variation we need only substitute for the number of absorbers $N_A(z)$ in terms of the polarization which in turn depends upon R. $N_A(z)$ is just the number of Rb atoms in the $|S,-\rangle$ state, N_S^-, and this can be related to the polarization P_{Rb} as $N_S^-=N_{Rb}(1+P_{Rb})/2$. Substituting this into Eq. (20) and rearranging to solve for dz we arrive at

$$dz=\frac{-dI(r,z)}{I(r,z)}\,\frac{2}{\hbar\omega_0\kappa N_{Rb}}\,\frac{1}{1+P_{Rb}}. \tag{22}$$

Now consider the average polarization that will be measured in an experiment over a macroscopic sample. We define this as $\overline{P_{Rb}}$ which is given by

$$\overline{P_{Rb}}=\frac{2\pi}{\pi r^2 l}\int_0^l\int_0^r P_{Rb}(z,r)r\,dr\,dz. \tag{23}$$

Neglecting P_{Rb}^0 the integration of $P_{\mathrm{Rb}}(z,r)$ over the length of the sample can be greatly simplified by changing the variables in Eq. (23) to an integration over the laser intensity using Eq. (22),

$$\overline{P_{\mathrm{Rb}}}=\frac{4}{3r^2 l\hbar\omega_0 N_{\mathrm{Rb}}\epsilon}\int_0^r\int_{I(0,r)}^{I(l,r)} dI r dr$$

$$=\frac{4}{3r^2 l\hbar\omega_0 N_{\mathrm{Rb}}\epsilon}\int_0^r [I(l,r)-I(0,r)] r dr. \tag{24}$$

Equation (24) demonstrates that the average steady state Rb polarization depends primarily upon the amount of laser intensity absorbed over the length of the sample. Essentially this is a power balance. Once polarized, the sample dissipates a certain amount of energy per unit time via spin lattice relaxation. To maintain this polarization this power must be provided by the laser beam thereby reducing its net intensity.

The remaining radial integral shown in Eq. (24) can be solved analytically if a functional form for the loss in laser intensity across the sample can be obtained from Eq. (22). Unfortunately, the general solution to Eq. (22) gives a transcendental form that cannot be inverted to simply give $I(l,r)$. If the sample is not being pumped efficiently, Eq. (22) reduces to Beer's law as expected. However, when pumping occurs, the light intensity decays linearly with distance into the sample,

$$I(l,r)-I(0,r)\approx -\frac{3l\hbar\omega_0 N_{\mathrm{Rb}}\epsilon}{2\left[1+\dfrac{3\epsilon}{\kappa I(0,r)}\right]}. \tag{25}$$

This equation can be recast directly in terms of r, by defining the incident laser intensity as a normalized Gaussian with a half-width designated by d,

$$I(0,r)=\frac{P_0}{\pi d^2}\ln(2)e^{-(r^2/d^2)\ln(2)},$$

where

$$\int_0^{2\pi}\int_0^{\infty} I(0,r) r dr d\phi = P_0. \tag{26}$$

Inserting this definition into Eq. (25) produces

$$I(l,r)-I(0,r)=\frac{-3l\hbar\omega_0 N_{\mathrm{Rb}}\epsilon}{2[1+\Delta e^{(r^2/d^2)\ln(2)}]},$$

where

$$\Delta=\frac{3\pi d^2\epsilon}{\kappa P_0\ln(2)}. \tag{27}$$

The dimensionless variable Δ has special significance. It is essentially the ratio of the rate per unit volume at which the sample can dissipate energy, 3ϵ, to the rate at which it is being absorbed, $\kappa P_0\ln(2)/\pi d^2$.

The linear expression is valid only for values of r and l where the laser intensity remains greater than zero. The positions in the sample where this expression gives $I(l,r)=0$ can be described as a critical boundary. Calculation of the critical boundary from Eq. (27) using typical experimental parameters indicates it typically lies outside the actual sample dimensions. This means that the approximation used to derive Eq. (27) is a good one for describing the experimental situation encountered in the laboratory. Since this is the case, the radial integral in Eq. (24) can be rewritten using Eq. (27) as

$$\overline{P_{\mathrm{Rb}}}=\frac{1}{r^2}\int_0^r\frac{-2r dr}{1+\Delta e^{(r^2/d^2)\ln(2)}}$$

$$=\frac{d^2}{r^2\ln(2)}\ln\left[\frac{e^{-(r^2/d^2)\ln(2)}+\Delta}{1+\Delta}\right]. \tag{28}$$

The expression for $\overline{P_{\mathrm{Rb}}}$ above can be recast in a more useful form by approximating $\ln(x)$ as $2(x-1)/(x+1)$ since the argument inside the natural log function is never larger than 1. Applying this approximation to Eq. (28) gives

$$\overline{P_{\mathrm{Rb}}}\approx\frac{2d^2}{r^2\ln(2)}\left[\frac{e^{-(r^2/d^2)\ln(2)}-1}{e^{-(r^2/d^2)\ln(2)}+2\Delta+1}\right]. \tag{29}$$

Taking the inverse of both sides of this equation we arrive at a linear relationship between the inverse polarization and the inverse laser power,

$$\text{where}\quad m=\frac{3\pi r^2\epsilon}{\kappa}\left[\frac{1}{e^{-(r^2/d^2)\ln(2)}-1}\right]$$

$$\frac{1}{\overline{P_{\mathrm{Rb}}}}=\frac{m}{P_0}+b, \tag{30}$$

$$\text{and}\quad b=\frac{r^2\ln(2)}{2d^2}\left[\frac{e^{-(r^2/d^2)\ln(2)}+1}{e^{-(r^2/d^2)\ln(2)}-1}\right].$$

When the laser beam width is larger than the sample diameter, $d\gg r$, Eq. (30) reduces to $1/|P_{\mathrm{Rb}}|=\Delta+1$. In this instance as the applied laser power $P_0\to\infty$, $\Delta\to 0$, and the absolute value of the Rb polarization goes to 1 as expected. For very small beam diameters, $r\gg d$, the intercept b becomes $r^2\ln(2)/2d^2$. In this case, the ultimate polarization that can be achieved is limited by the overlap of the laser beam and the sample cross sectional areas.

For comparison with experiment it is actually more useful to consider the signal or magnetization M_{Xe}, and its dependence upon P_0. This signal will be directly proportional to the polarization shown in Eq. (30). Taking this proportionality to be $M_{\mathrm{Xe}}=aP_{\mathrm{Rb}}$ ($\gamma\approx 1$), the following volume averaged ^{129}Xe signal can be obtained:

$$\frac{1}{M_{\mathrm{Xe}}}=\frac{1}{aP_{\mathrm{Rb}}}=\left(\frac{m}{a}\right)\frac{1}{P_0}+\frac{b}{a}. \tag{31}$$

This result provides for a very useful approach to measuring the polarization efficiency of an experimental setup from the laser power dependence of the ^{129}Xe NMR signal. In general, a direct NMR measurement of the ^{129}Xe polarization is difficult, as it requires that the signal intensity corresponding to unpumped ^{129}Xe in the absence of Rb be known. This taxes the dynamic range of the spectrometer, and is made more difficult by long T_1^{Xe}'s.[13] Equation (31) suggests an alternative approach. The inverse of the signal $1/M_{\mathrm{Xe}}$ is

plotted vs the inverse of the laser power $1/P_0$. Taking the slope to intercept ratio from the plot gives m/b since a divides out,

$$\frac{m}{b}=\frac{6\pi\epsilon d^2}{\kappa\ln(2)}\left[\frac{1}{e^{-(r^2/d^2)\ln(2)}+1}\right]. \tag{32}$$

When $r\gg d$, the m/b ratio becomes $m/b=6\pi\epsilon d^2/\kappa\ln(2)$. This ratio in the small sample diameter limit, $r\ll d$, reduces to half this value, i.e., $m/b=3\pi\epsilon d^2/\kappa\ln(2)$. Since b is determined only by the laser beam diameter and the sample radius, m can be determined from the experimentally determined value for m/b. With m, b, and a determined, the polarization can be calculated at any given laser power level. This approach to determining a ^{129}Xe polarization is much less prone to experimental error (or wishful thinking) than other methods. Since m itself is determined by sample composition, r, d, T_1^{Xe}, and T_1^{Rb}, measurement of the pertinent relaxation times provides an internal consistency check. Alternatively, the determination of m may be used to measure ϵ and thus provide a means of estimating one of the relaxation parameters.

D. Effect of different photon polarizations

The above treatment is appropriate in the limit that there are no photons of other polarizations or wavelengths capable of pumping the other three transitions in the Rb D_1 line. Recall that the D_1 line consists of four transitions in high magnetic field as shown in Fig. 2. The two π transitions occur in energy between the σ_+ and σ_- lines. The highest energy transition is produced by the absorption of σ_+ light, while the lowest energy transition occurs with σ_- light. When the optical resonances are narrow and the magnetic field is high, depolarization of the pumping beam translates into a decrease in useful applied laser power. In this case photons of only one polarization may be absorbed for any one optical resonance condition. Therefore, low pressure cells may be pumped with randomly polarized light in a high enough magnetic field, albeit at 1/4 the power efficiency possible with a single light polarization. In this limit, the other photon polarizations are seen as being significantly off resonance of the other transitions.

In experiments where high pressures of ^{129}Xe buffer gas are employed the situation is somewhat different. In this case the buffer gas broadens the optical lines (typically $\Delta_{1/2}/2\pi\sim 80$ GHz at $P\sim 1$ atm). Consequently, all photon polarizations are somewhat capable of pumping the D_1 line since the spectral dispersion afforded by the high magnetic field has been washed out. The efficacy of pumping by the different types of photons present will depend upon the intensity of each pressure broadened transition's line shape at the applied laser frequency.

To realistically model spin exchange pumping in the laboratory it is necessary to include the effects of the photons at the unwanted polarizations. The way this is accomplished is by first realizing that the total number of photons impinging on the sample is an experimentally set constant, which gives rise to a total pumping rate, r_T. In the previous section, all of the photons were treated as being ''useful,'' i.e., we considered them as essentially being dumped into only the transition that is selected by both laser wavelength and polarization giving $r_T=R$. In the case now considered, all of the photons are not just connecting one transition. They are instead spread out unevenly among the four D_1 absorptions. This gives rise to four different pumping rates, r_{nm}, designated by the magnetic sublevels connected by the laser in the ground, n, and excited, m, states. The pumping rate for a given transition, r_{nm}, is the product of the overlap between the laser line and that particular pressure broadened atomic absorption, κ_{nm}, and the intensity of the light capable of driving the transition, I_{nm}, i.e., $r_{nm}=\kappa_{nm}I_{nm}$.

Transition	Rate
$\lvert S,-\rangle\rightarrow\lvert P,+\rangle$	$r_{-+}=\kappa_{-+}I_{-+}$
$\lvert S,+\rangle\rightarrow\lvert P,+\rangle$	$r_{++}=\kappa_{++}I_{++}$
$\lvert S,-\rangle\rightarrow\lvert P,-\rangle$	$r_{--}=\kappa_{--}I_{--}$
$\lvert S,+\rangle\rightarrow\lvert P,-\rangle$	$r_{+-}=\kappa_{+-}I_{+-}$.

(33)

The κ_{nm} factors differ in size by the overlap between the laser line and the $n\rightarrow m$ optical absorption and the angular momentum selection rule for that particular transition, i.e., $\kappa_{nm}=(|n-m|+1)B_{12}\Omega_{nm}/3c$. An analytical form for the four Ω_{nm}'s can be obtained by taking the atomic frequency response as a pressure broadened Lorentzian line shape centered at ω_{nm} and the laser line as a delta function centered at the applied laser frequency, ω_L,

$$\Omega_{nm}=\frac{2\Delta_{1/2}}{\pi[4(\omega_L-\omega_{nm})^2+\Delta_{1/2}^2]}. \tag{34}$$

It is clear from Eq. (34) that Ω_{nm} has inverse angular frequency units. As mentioned above the total laser intensity impinging on the sample can be separated into four components, I_{nm}, on the basis of optical polarization. Since the total laser intensity is constant the I_{nm}'s are linearly related to the total intensity by four factors, a_{nm}, whose sum is normalized to 1, $I_{nm}=a_{nm}I$.

Before calculating the effects of random photon polarizations on P_{Rb} using rate theory, it is useful to group the $\Omega_{nm}a_{nm}$ products into four new factors that are useful for comparison to experiment. The maximum polarization, $P_{\mathrm{Rb}}^{\max}$, and the total pumping rate, r_T, are just straight sums and differences of the $\Omega_{nm}a_{nm}$'s,

$$P_{\mathrm{Rb}}^{\max}=\frac{\Omega_{++}a_{++}+\Omega_{+-}a_{+-}-\Omega_{-+}a_{-+}-\Omega_{--}a_{--}}{\Omega_{++}a_{++}+\Omega_{+-}a_{+-}+\Omega_{-+}a_{-+}+\Omega_{--}a_{--}},$$

$$r_T=\frac{2B_{12}}{3c}(\Omega_{++}a_{++}+\Omega_{+-}a_{+-}+\Omega_{-+}a_{-+}+\Omega_{--}a_{--})I=\frac{2B_{12}}{3c}pI=\kappa_T I, \tag{35}$$

where κ_T is the total intensity removed from the laser per second. The light attenuation factor, Q, and the total attenuation, q, of the laser beam are similar to $P_{\mathrm{Rb}}^{\max}$ and p, differ-

ing only in the inclusion of weighting factors determined by the angular momentum selection rules for the $n \rightarrow m$ transition,

$$Q = \frac{\Omega_{++}a_{++} + 2\Omega_{+-}a_{+-} - 2\Omega_{-+}a_{-+} - \Omega_{--}a_{--}}{\Omega_{++}a_{++} + 2\Omega_{+-}a_{+-} + 2\Omega_{-+}a_{-+} + \Omega_{--}a_{--}},$$
$$q = \Omega_{++}a_{++} + 2\Omega_{+-}a_{+-} + 2\Omega_{-+}a_{-+} + \Omega_{--}a_{--}. \tag{36}$$

It is important to notice that if $L=0$ in the doublet excited state instead of $L=1$, then $P_{\mathrm{Rb}}^{\max}=Q$ and $p=q$ as the angular momentum selection rules for all of the transitions would be identical and equal to 1/2. When spectral dispersion is maintained, be it by low buffer gas pressure or high magnetic field and only σ_+ photons are present, tuning the laser to the σ_+ transition gives $P_{\mathrm{Rb}}^{\max}=-1$ and $r_T=R$. However, in the usual case where pressure broadening is significant, the rates connecting each of the four D_1 transitions must be considered. In this situation, the $|S,-\rangle \rightarrow |P,+\rangle$ transition rate decreases from $R=\kappa I$ to $r_{-+}=\kappa_{-+}I_{-+}$ due to the other photon polarizations in the sample. The effect of these three additional rates on the optical pumping cycle in Rb can be obtained by writing down the rate equations appropriate for the four level system shown in Fig. 2. The major difference thus far between the treatment in this section and the earlier one is the inclusion of the additional rates connecting the previously neglected excited state magnetic sublevel, $|P,-\rangle$, to the other three states. The Rb polarization, P_{Rb}, is found in the same way as above using exactly the same definitions for $R_{\mathrm{Rb}}\downarrow$ and $R_{\mathrm{Rb}}\uparrow$. In the usual limit that A is considered as infinite P_{Rb} is

$$P_{\mathrm{Rb}} = \frac{R_{\mathrm{Rb}}\downarrow - R_{\mathrm{Rb}}\uparrow + \frac{1}{3}P_{\mathrm{Rb}}^{\max}r_T}{R_{\mathrm{Rb}}\downarrow + R_{\mathrm{Rb}}\uparrow + \frac{1}{3}r_T}. \tag{37}$$

This equation can also be obtained from Eq. (4) by replacing AN_P^+ with RN_S^-, $R_{\mathrm{Rb}}\uparrow$ with $R_{\mathrm{Rb}}\uparrow+(2r_{--}+r_{-+}-R)/3$ and $R_{\mathrm{Rb}}\downarrow$ with $R_{\mathrm{Rb}}\downarrow+(2r_{++}+r_{+-})/3$. Paralleling the previous section throughout the remainder of the calculation, we first determine P_{Rb} in the presence of a spinless buffer gas where the same definitions for P_{Rb}^0 and T_1^{Rb} shown in Eq. (11) have been used,

$$P_{\mathrm{Rb}} = \frac{P_{\mathrm{Rb}}^0 + \frac{1}{3}P_{\mathrm{Rb}}^{\max}r_T T_1^{\mathrm{Rb}}}{1 + \frac{1}{3}r_T T_1^{\mathrm{Rb}}}. \tag{38}$$

Comparison to Eq. (8) reveals that a mixture of photons with differing polarization simply results in a smaller ultimate achievable Xe polarization $P_{\mathrm{Rb}}^{\max}$.

The effect of photons having different polarizations on the pumping of the Xe gas due to spin exchange with polarized Rb can likewise be derived. In most instances the spontaneous emission rate, A, can be considered as being infinite in comparison to the other rates during the optical pumping cycle. All that must be considered then are the S state spin populations for Rb and the two populations of the ^{129}Xe nuclear spin states. Replacement of $W_{\mathrm{Rb}}\uparrow+R/3$ with $W_{\mathrm{Rb}}\uparrow+(2r_{--}+r_{-+})/3$ and $W_{\mathrm{Rb}}\downarrow$ with $W_{\mathrm{Rb}}\downarrow+(2r_{++}+r_{+-})/3$ in each instance in Eqs. (10) give the time rate of change of N_S^- and N_{Xe}^- when all photon polarizations are present. Proceeding in exactly the same way as before gives the Rb polarization during spin exchange with ^{129}Xe and optical pumping in the thin sample limit,

$$P_{\mathrm{Rb}} = \frac{P_{\mathrm{Rb}}^{\max} + \frac{3\epsilon}{r_T}P_{\mathrm{Rb}}^0}{1 + \frac{3\epsilon}{r_T}}. \tag{39}$$

When the available photons are purely σ_+ polarized, $P_{\mathrm{Rb}}^{\max}\rightarrow -1$, $r_T \rightarrow R$, and Eq. (17) is obtained. In the usual case though some depolarization is present giving $|P_{\mathrm{Rb}}^{\max}|<1$, and Eq. (36) is more applicable.

Unfortunately the thin sample limit is rarely encountered in the laboratory, and calculation of the volume averaged Rb polarization when all photon polarizations are present is somewhat more complex. As a starting point, we again use the fact that the total laser intensity, I, is divided into four separate intensities, I_{nm}, on the basis of the four optical polarizations, i.e., two π and one each σ_+ and σ_-. In order to determine the loss in total laser intensity, dI, across the sample we must first consider the attenuation of each component of I separately. This treatment leads to four coupled differential equations describing the beam attenuation,

$$dI_{-m} = -\hbar\omega_0 N_S^- \kappa_{-m} I_{-m} dz \quad \text{and} \quad dI_{+m} = -\hbar\omega_0 N_S^+ \kappa_{+m} I_{+m} dz. \quad \text{where } m = + \text{ or } - \tag{40}$$

The top set of equations is due to absorption by the Rb atoms in N_S^- while the lower set is due to those in N_S^+. The loss in total laser intensity across the sample can be written using the definitions of P_{Rb}, $P_{\mathrm{Rb}}^{\max}$, r_T, p, and q shown in Eqs. (35), (36), and (38),

$$dI = \sum_{n,m} dI_{nm} = -\frac{\hbar\omega_0 N_{\mathrm{Rb}} q}{4p}\left[\frac{r_T(1-QP_{\mathrm{Rb}}^{\max})+3\epsilon}{1+\frac{3\epsilon}{r_T}}\right]dz. \tag{41}$$

The average Rb polarization across the sample, $\overline{P_{\mathrm{Rb}}}$ is defined in exactly the same way as before. Equation (41) is used to recast the average over length to an average over laser intensity,

$$\overline{P_{\mathrm{Rb}}}=\frac{-4}{r^2 l\hbar\omega_0 N_{\mathrm{Rb}}} \times\int_0^r\int_{I(0,r)}^{I(l,r)}\frac{P_{\mathrm{Rb}}^{\max}}{3\epsilon+(1-QP_{\mathrm{Rb}}^{\max})\kappa_T I}\,dI\;\;rdr$$

$$=\frac{-4}{r^2 l\hbar\omega_0 N_{\mathrm{Rb}}\kappa_T}\left(\frac{P_{\mathrm{Rb}}^{\max}}{1-QP_{\mathrm{Rb}}^{\max}}\right) \times\int_0^r \ln\left[\frac{3\epsilon+(1-QP_{\mathrm{Rb}}^{\max})\kappa_T I(l,r)}{3\epsilon+(1-QP_{\mathrm{Rb}}^{\max})\kappa_T I(0,r)}\right]rdr. \tag{42}$$

Notice again that when all of the photons are σ_+ polarized and on resonance with the σ_+ transition, $P_{\mathrm{Rb}}^{\max}$ and $Q\rightarrow -1$ while $\kappa_T\rightarrow\kappa$. In this case the usual average and laser intensity variation shown in Eqs. (22) and (24) are obtained. The remaining radial integral shown in Eq. (42) has no simple analytical solution. Approximating the integrand using $\ln(x)\approx x-1$ gives

$$\overline{P_{\mathrm{Rb}}}=\frac{-4P_{\mathrm{Rb}}^{\max}}{r^2 l\hbar\omega_0 N_{\mathrm{Rb}}}\int_0^r\frac{[I(l,r)-I(0,r)]rdr}{3\epsilon+(1-QP_{\mathrm{Rb}}^{\max})\kappa_T I(0,r)}. \tag{43}$$

As before, no simple analytical solution for $I(l,r)$ can be obtained from Eq. (41), so we again obtain an approximate form using a series expansion of the natural log term. Rearrangement of this equation gives $I(l,r)-I(0,r)$ as

$$I(l,r)-I(0,r)\simeq\frac{-l\hbar\omega_0 N_{\mathrm{Rb}} q\kappa_T}{4p\left[\dfrac{1}{I(0,r)}+\dfrac{QP_{\mathrm{Rb}}^{\max}\kappa_T}{3\epsilon+(1-QP_{\mathrm{Rb}}^{\max})\kappa_T I(0,r)}\right]}. \tag{44}$$

Taking the limits of Eqs. (43) and (44) when $P_{\mathrm{Rb}}^{\max}$ and $Q\rightarrow -1$, $\kappa_T\rightarrow\kappa$, and $q\rightarrow 2p\rightarrow\Omega$ shows that they properly reduce to the previous expressions obtained in Eqs. (24) and (25). Inserting Eq. (44) into Eq. (43) and using the definitions for $I(0,r)$ and Δ from earlier gives

$$\overline{P_{\mathrm{Rb}}}=\frac{q}{pr^2}\int_0^r\frac{P_{\mathrm{Rb}}^{\max}rdr}{1+\dfrac{\kappa}{\kappa_T}\Delta e^{(r^2/d^2)\ln(2)}}$$

$$=\frac{-P_{\mathrm{Rb}}^{\max}qd^2}{2pr^2\ln(2)}\ln\left[\frac{e^{-(r^2/d^2)\ln(2)}+\dfrac{\kappa}{\kappa_T}\Delta}{1+\dfrac{\kappa}{\kappa_T}\Delta}\right]. \tag{45}$$

As in the previous section, Eq. (45) can ultimately be rearranged to give a relationship between the inverse polarization and inverse laser power,

$$\frac{1}{P_{\mathrm{Rb}}}=\frac{m'}{P_0}+b',\quad\text{where}\quad m'=\frac{-2p\kappa}{P_{\mathrm{Rb}}^{\max}q\kappa_T}m,\quad b'=\frac{-2p}{P_{\mathrm{Rb}}^{\max}q}b \tag{46}$$

where m and b are defined by Eq. (30).

The result shown above in Eq. (46) parallels that in Eq. (31). Again, a plot of the inverse signal as a function of the inverse laser power should be linear. In this case, one can see that the presence of other photon polarizations will scale the slope to intercept ratio by a depolarization factor κ/κ_T. Comparison of the calculated m/b to the apparent experimental value then gives a measure of laser light depolarization for comparison to optical results.

To use the expressions generated above to model an optical pumping experiment, one must be able to experimentally estimate both the Ω_{nm} and a_{nm} factors. In our experimental setup laser linewidth is on the order of 2 GHz, which is much narrower than the pressure broadened atomic absorption line widths in atmosphere pressure cells ($\Delta_{1/2}/2\pi\sim 80$ GHz). In this case values for the four Ω_{nm}'s can be directly calculated from Eq. (34). The fraction of total light intensity pumping an $n\rightarrow m$ transition, a_{nm}, as well as the width of each line, $\Delta_{1/2}$, can be obtained from the high field optical spectra of the Rb D_1 absorption.

Examples of how $P_{\mathrm{Rb}}^{\max}$ and κ/κ_T from one experimental situation to another are easily examined. The situation where only σ_+ polarized light on resonance with the σ_+ transition has been mentioned repeatedly throughout this section. The line intensities listed in order of decreasing energy as shown in Fig. 2 for this situation are 1:0:0:0. This gives $a_{-+}=1$ while setting the other three a_{nm}'s to zero. Calculating $P_{\mathrm{Rb}}^{\max}$ and κ/κ_T from Eqs. (34) and (35) gives -1 and 1, respectively. This should be expected upon comparison with the equations developed in the previous section for only σ_+ light. When partially depolarized light is present the situation is a bit different. Consider an optical spectrum having linewidths of $\Delta_{1/2}/2\pi=80$ GHz due to pressure broadening from $\sim$1 atm of Xe gas and line intensities again listed in order of decreasing energy of 1:.59:.65:.71. This reduces the σ_+ intensity factor to $a_{-+}=.34$ while increasing the other three terms to $a_{++}=0.20$, $a_{--}=0.22$, and $a_{+-}=0.24$. Calculating the appropriate overlap factors, Ω_{nm}, from Eq. (34) allows the calculation of $P_{\mathrm{Rb}}^{\max}=-0.66$ and $\kappa/\kappa_T=2.05$ at $B_0=2.35$ T from Eq. (35). One other experimental situation of interest demonstrates the advantage of the spectral dispersion afforded by the high magnetic field on the production of polarized Xe gas. Optical pumping with randomly polarized light having 1:1:1:1 spectral intensities forces all four a_{nm}'s to be the same and equal to 1/4. In this case $P_{\mathrm{Rb}}^{\max}$ decreases to -0.6 and κ/κ_T increases to 2.36. Notice that if a high magnetic field were not insured no spin polarization could be produced as the four Ω_{nm}'s would be equal to Ω and all of the D_1 lines in Rb would be pumped at their maximum respective rates.

E. Other leakage mechanisms

The treatment outlined to this point is appropriate for the situation when only Rb–^{129}Xe mixtures are used. This is the case when isotopically pure ^{129}Xe gas is available. In some instances, however, one may want to use natural abundance Xe gas having a 26.44% ^{129}Xe and 21.18% ^{131}Xe isotopic mixture. ^{131}Xe is an $I=3/2$ nucleus, and in the gas phase where the effects of its quadrupole moment are motionally averaged, has four equally spaced energy levels. The theory

outlined above for Rb–^{129}Xe spin exchange optical pumping is easily applied to the Rb–^{131}Xe case, and the same sort of equations result. These equations show that the effect of the ^{131}Xe nucleus on P_{Rb} shown in Eq. (17) is to augment the leakage relaxation factor, ϵ. When ^{131}Xe is present, ϵ can be rewritten in terms of the ^{131}Xe number density, N_{XQ}, relaxation time, T_1^{XQ}, and spin exchange time, $T_{1,Q}^{\mathrm{se}}$, as

$$\epsilon=\frac{1}{T_1^{\mathrm{Rb}}}+\frac{\alpha\gamma}{T^{\mathrm{Xe}}}+\frac{\alpha_Q\gamma_Q}{T_1^{XQ}},\quad \text{where}\quad \alpha_Q=\frac{N_{XQ}}{N_{\mathrm{Rb}}}\quad \gamma_Q=\frac{5}{1+\dfrac{T_{1,Q}^{\mathrm{se}}}{T_1^{XQ}}}. \tag{47}$$

As mentioned before, the $\alpha\gamma/T_1^{\mathrm{Xe}}$ term represents a depolarization of the Rb via leakage through the relaxation of the ^{129}Xe. This in turn limits how high the polarizations can be for a given laser power. The $\alpha_Q\gamma_Q/T_1^{XQ}$ term is also a leakage rate, and in certain cases, as will be discussed below, can be quite large. A similar term, $\alpha_N\gamma_N/T_1^N$, is operative for leakage relaxation via the ^{14}N nuclei in the N_2 buffer gas component commonly added to pumping cells of this type.

III. EXPERIMENT

A. Cell preparation

Two types of sample containers were used in these experiments. One will be referred to as a ''torpedo cell'' which is just a cylindrical Pyrex tube having one flat closed end approximately 7 cm long and 9 mm in diameter. The other sample holder will be referred to as a ''high quality'' optical container and is a 5 cm long 1 in. diam tube with optical windows fused to either end. The open end of the torpedo cell is fused to a 5 cm long 3/8 in. diam tube. The high quality optical cell has a 5 cm long 3/8 in. diam tube connected directly to the side of the 1 in. glass cell. The 3/8 in. diam tubes in each instance are used both to admit Rb and Xe into the cells and to connect the cells to a vacuum manifold as discussed below. Each container is filled with Ultra-Pure water and sonicated for 20 min in order to remove paramagnetic ions from the inner surfaces. Each cell is baked at 140 °C for ≈12 h, coated with a 10% Surfasil Siliconizing Fluid/dry pentane mixture and attached to one end of a teflon stopcock with a 3/8 in. Cajon fitting. The other end of the stopcock is then mounted on a vacuum rack using a 14/20 ground glass joint. The stopcock is opened to the vacuum manifold and the cell is evacuated to 10^{-4} Torr for ≈1 h in order to remove any excess pentane. Following this pumping period, the stopcock is closed and the evacuated cell/stopcock combination is removed from the vacuum rack and placed in a glove box containing a N_2 atmosphere. The cell is released from the stopcock by loosening the Cajon fitting and a visible amount of natural isotopic abundance Rb metal is pipetted into it. The cell is reattached to the stopcock with the Cajon fitting, removed from the glove box and remounted on the vacuum rack via the 14/20 ground glass joint. The stopcock is opened once more and the cell is evacuated to 10^{-4} Torr for ≈1 h. The cell is then charged to the appropriate amount with Spectra Gasses 99.999% Xe and stock grade N_2 buffer gas. Pressure measurements were made using an Omega 136PC15a2 9234 pressure transducer attached to an Omega DP 2000 Omegarometer. The torpedo cell is then sealed to a length of ≈5 cm measured from the flat closed end using a torch and removed from the vacuum manifold. The high quality optical container is sealed as close as possible to the 1 in. container body with a torch and removed from the vacuum manifold.

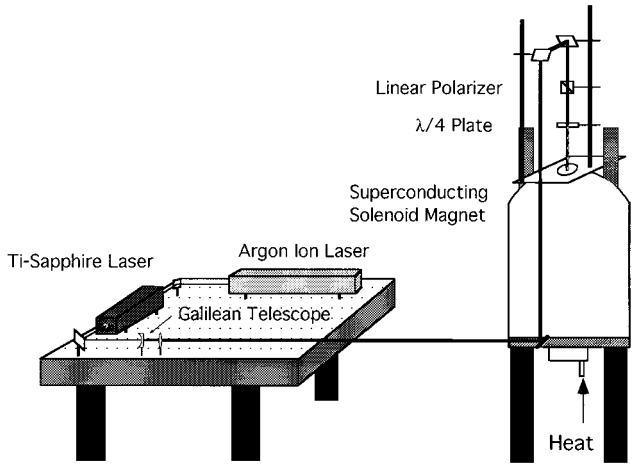

FIG. 3. Experimental setup showing the polarization of nuclear spins in high magnetic fields based on an Oxford superconducting solenoid and a Coherent Ti–sapphire ring laser.

B. Optical apparatus and spectroscopy

Optical spectroscopy is accomplished in high magnetic fields (B_0=2.35 T and 7.04 T) as shown in Fig. 3. Infrared laser light (λ=794.74 nm) is produced by a Coherent Model 899 Ti-sapphire ring laser pumped by a Spectra Physics Model 164 Argon Ion Laser. A Quanta Ray MCI-1 controller drives a Superior Electric Slo-Syn synchronous stepper motor attached to the ring laser in order to wavelength scan in increments of 0.02 nm. A small portion of the output of the ring laser is directed into a Burleigh WA-20VIS wavemeter for wavelength measurement while the remainder is expanded to the desired Gaussian beam diameter with a Galilean Telescope. This light is elevated approximately 1 m to the top of either an Oxford Instruments 7.04 T 89 mm room temperature bore or 2.35 T 110 mm room temperature bore superconducting solenoid magnet. All reflections are made at 90° in order to maximize the linear polarization produced by the laser. The laser beam is then directed into a linear polarizer, a λ/4 plate when circularly polarized light is needed, and finally into a magnetic resonance probe containing one of the cells. The homebuilt magnetic resonance probe suspends the cell in a Helmholtz coil enclosing a volume of ≈2 cm^3 and tuned to the appropriate Larmor frequency for ^{129}Xe. The coil and sample are contained in a Teflon oven that permits laser illumination and heating via hot air (<150 °C) produced by blowing cold air over an Omegalux tubular heater. In the case of the torpedo cell, light is admit-

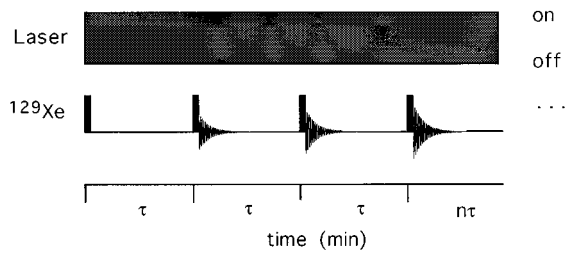

FIG. 4. Magnetic and optical resonance pulse sequence used to monitor the temporal buildup of nuclear spin polarization during the optical pumping process. Each duration τ is on the time scale of minutes.

ted through the flat closed end while for the high quality optical cell it is through the optical windows. Monitoring of optical transitions in the bore of the superconducting solenoid magnet is accomplished via a fiberoptic connected to a photodiode. The laser is tuned to the D_1 resonance line in Rb by adjusting the laser wavelength and monitoring voltage fluctuations from the photodiode with an oscilloscope. Laser power measurements were accomplished using a Coherent Model 200 power meter. Laser beam diameter measurements were done by chopping the laser beam with a micrometer and recording the decrease in laser power. A fit of this data to an error function provides the Gaussian laser beam diameter.

C. Magnetic resonance spectroscopy

All magnetic resonance spectra are obtained on home-built NMR spectrometers constructed around either a Nicolet Analytical Instruments Model 1280 data acquisition system for experiments at 2.35 T or a TecMag Libra data acquisition system for experiments at 7.04 T. 90° radio frequency pulses are calibrated using the ^{81}Br resonance in solid KBr.

Measurement of the steady state ^{129}Xe signal at various laser powers, $M_{\mathrm{Xe}}(P_0,\infty)$, was accomplished in separate ways depending on whether a short $T_1^{\mathrm{Xe}*}$ was present. In all cases the buildup of ^{129}Xe signal, $M_{\mathrm{Xe}}(P_0,t)=aP_{\mathrm{Xe}}$, during optical pumping with laser power P_0 is a single exponential process,

$$M_{\mathrm{Xe}}(P_0,t)=M_{\mathrm{Xe}}(P_0,\infty)[1-e^{-(t/T_1^{\mathrm{Xe}*})}]. \tag{48}$$

When a short $T_1^{\mathrm{Xe}*}$ was present the measurement of $M_{\mathrm{Xe}}(P_0,\infty)$ was obtained from characterization of the full signal growth curves at various choices of P_0. Under these conditions the gain in signal can be experimentally monitored by periodically sampling a portion of $M_{\mathrm{Xe}}(P_0,t)$ with a small tip angle rf pulse as shown in Fig. 4. In the experimental setup, the magnetic resonance coil does not enclose the entire sample volume. As long as τ is longer than the atomic self-diffusion time, the detection of $M_{\mathrm{Xe}}(P_0,t)$ will be independent of the fraction of the total magnetization sampled. Since $\tau \gg T_2^{\mathrm{Xe}}$, steady state spin echo phenomena are not important.[14] The observed signal's temporal gain in intensity then becomes a direct measure of $M_{\mathrm{Xe}}(P_0,t)$ due to optical pumping. The experimentally detected ^{129}Xe signal as a function of the number of the pulse, n, is just a modified version of Eq. (48),

$$M_{\mathrm{Xe}}(P_0,n\tau)=M_{\mathrm{Xe}}(P_0,\infty)[1-e^{-(n\tau/T_1^{\mathrm{Xe}*})}]. \tag{49}$$

Fitting the data measured in this way to Eq. (48) provides $M_{\mathrm{Xe}}(P_0,\infty)$.

This type of measurement is not appealing when larger $T_1^{\mathrm{Xe}*}$'s are present. Instead, we measure and characterize just one growth curve as above to obtain $T_1^{\mathrm{Xe}*}$. Values of $M_{\mathrm{Xe}}(P_0,\infty)$ at various P_0's are then generated from a measurement of $M_{\mathrm{Xe}}(P_0,t=2\ \mathrm{min})$, Eq. (48), and $T_1^{\mathrm{Xe}*}$. When $T_1^{\mathrm{Xe}*}$'s on the order of 1 h are observed this method translates into a time savings of ~9 h when data points at ten different laser powers are necessary.

Full growth curves of the ^{129}Xe NMR signal were measured for the torpedo cell at both $B_0=2.35$ T and 7.04 T and at laser powers between 100 mW and 600 mW in 100 mW intervals. In each case the same torpedo cell having 484 Torr of Xe and 76 Torr of N_2 gases at a temperature of 110 °C was used. The length and inner radius of the sample tube were $l=5$ cm and $r=3$ mm, respectively while the Gaussian beam radius was $d=1$ mm in each instance.

Measurement of the full growth curves for the ^{129}Xe NMR signal were not possible at all laser powers in the high quality optical cell as $T_1^{\mathrm{Xe}*}$ was very long. Instead the ^{129}Xe signal was measured after 2 min of optical pumping for laser powers between 100 mW and 600 mW in 50 mW intervals. These experiments were done at $B_0=2.35$ T and $T=89$ °C. The signal was actually measured five separate times and the average value was obtained at a given P_0. This averaging process eliminates the noise present in the experiment such as variations in the cell temperature, laser power, and laser wavelength. These averaged signal intensities could be related to their steady state values by characterizing just one full growth curve to obtain $T_1^{\mathrm{Xe}*}$. The high quality optical cell contained 1 atm of Xe gas and was housed in a magnetic resonance probe designed to allow the laser beam to pass freely through the length of the bore of the superconducting solenoid magnet. The length and inner radius of the container were $l=5$ cm and $r=10.6$ mm, respectively while the Gaussian laser beam diameter was $d=2.7$ mm.

IV. RESULTS

Figure 5(a) shows the increase in ^{129}Xe signal as a function of laser power and n for the torpedo cell at $B_0=7.04$ T. In this experiment there is $\tau=1$ min between detected points. Similar curves not included here were also observed at $B_0=2.35$ T. The time constant of the pumping of ^{129}Xe, $T_1^{\mathrm{Xe}*}=3.45$ min at 110 °C, is constant for different incident laser intensities as determined by regressing the data to Eq. (48).

Figure 5(b) summarizes the behavior of the inverse signal, $1/M_{\mathrm{Xe}}(P_0,\infty)$, as a function of $1/P_0$ at $B_0=2.35$ T (triangles) and 7.04 T (diamonds) for the torpedo cell. The points shown in Fig. 5(b) have been scaled from the experimental data in each case in order to accommodate the curves

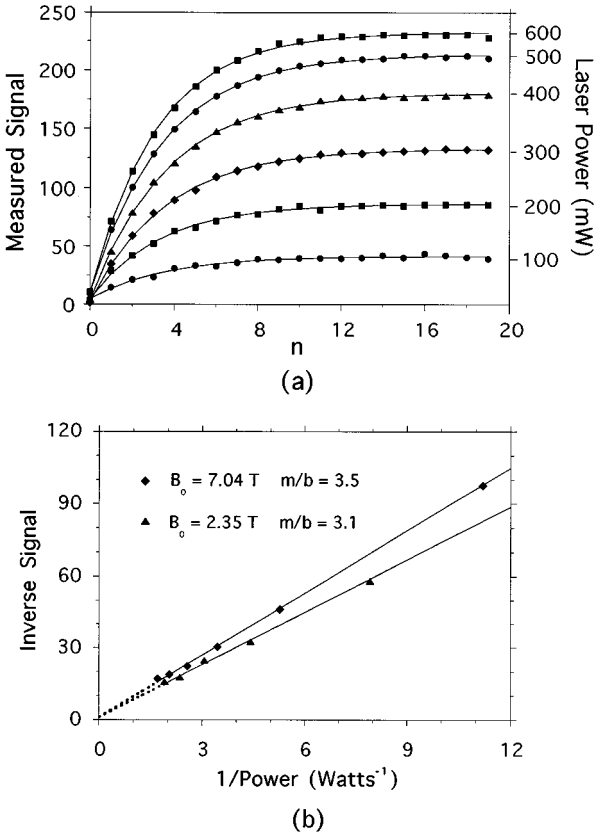

FIG. 5. (a) Temporal development of ^{129}Xe signal at 110 °C in a field of B_0=7.04 T as a function of incident laser power for a 1 mm diam laser beam. n represents one less than the number of the rf pulse as discussed in the text. This data was collected for a sample containing 684 Torr of ^{129}Xe and 76 Torr N_2 buffer gas. (b) Summary of the equilibrium pumped signal at both B_0=2.35 T (triangles) and 7.04 T (diamonds) as a function of the inverse laser power. The signals were scaled in each instance in order to fit them on the same set of axes. Notice that the inverse signal is linear with the inverse laser power as suggested by Eq. (31).

obtained at both field strengths on one plot. Equation (32) suggests that when a plot of $1/M_{\mathrm{Xe}}(P_0,\infty)$ vs $1/P_0$ is linear, and $r>d$, as is the case here, the slope/intercept ratio m/b should give $2\Delta P_0$. Experimental apparent values of $m/b(2.35\ \mathrm{T})=3.1$ W and $m/b(7.04\ \mathrm{T})=3.5$ W were obtained by linearly regressing the two data sets shown in Fig. 5(b).

The behavior of the inverse signal (triangles) as a function of the inverse laser power for the high quality optical container is shown in Fig. 6. The time constant of the ^{129}Xe polarization was found to be $T_1^{\mathrm{Xe}*}=43$ min at 89 °C as found from analysis of the full growth curve during optical pumping (not shown here). The slope to intercept ratio in this case was smaller than that seen in the torpedo cell, $m/b(2.35\ \mathrm{T})=0.3$ W, as determined by linearly regressing the data in Fig. 6.

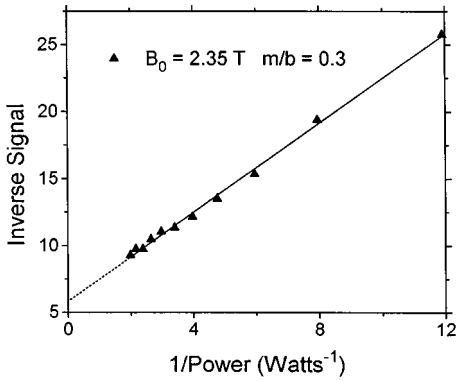

FIG. 6. Plot of the inverse signal as a function of the inverse laser power showing their linear relationship as measured in the high quality optical container (triangles) at B_0=2.35 T. Notice that the effects of unwanted photon polarizations are minimized with this sample container as can be seen by the smaller slope to intercept ratio in comparison to the data shown in Fig. 5.

V. DISCUSSION

The results outlined above for the torpedo cell are consistent with Eq. (10). The rate of polarization depends only on the number density of Rb, N_{Rb}, not on the laser intensity or power. Only the final magnetization, $M_{\mathrm{Xe}}(P_0,\infty)$, depends on the laser power as indicated by Eq. (28) and illustrated in Fig. 5(a).

The measured m/b values at the two field strengths for the torpedo cell compare rather poorly with the value calculated from Eq. (32), $m/b\approx 55$ mW, for $d=1$ mm, $\Delta_{1/2}/2\pi=80$ GHz, $B_{12}=6.45\times10^{21}$ (rad m^3/s)/(J s), and $\epsilon=36\,623\ \mathrm{s}^{-1}$ (the relaxation times used to calculate ϵ will be discussed below). The difference in m/b between experiment and theory can largely be reconciled by realizing that the laser beam is not allowed to freely exit the sample. The beam actually scatters off the back of the torpedo sample which randomizes the photon polarization and puts measurement of the beam diameter, $2d$, in question. Measurement of the Rb optical spectra in these torpedo cells in high B_0 will be discussed elsewhere.[15] That study showed that even when σ_+ light was used the high field optical spectrum of the Rb D_1 absorption had four lines in a 1:0.59:0.65:0.71 intensity ratio listed in order of decreasing energy. It was shown above that this optical spectrum gives $P_{\mathrm{Rb}}^{\max}=-0.66$ and $\kappa/\kappa_T=2.05$ when pressure broadened atomic lines having $\Delta_{1/2}/2\pi\approx 80$ GHz are present. Calculation of m'/b' from Eq. (46) under these less than optimal optical conditions using the same parameters as above gives $m'/b'=3.3$ W when $d=7.5$ mm. This unexpectedly large effective beam radius can be justified by an experimental observation of the light emitted from the torpedo cell outside the superconducting magnet with an IR viewer. At low laser powers, the laser beam is not intense enough to penetrate completely through the sample and just low intensity fluorescent light is observed from cell. Increasing the laser power further, into the regime where these experiments were accomplished, causes the beam to fall on the rear of the cell and scatter in all directions. A corresponding jump in light intensity in all directions from the rear of the cell is then detected by the IR viewer. This reflected beam is essentially randomly polarized and has a much larger divergence and radius than the input beam. In order to take this observation into account, model-

ing the experimental data from the torpedo cells requires a smaller $P_{\mathrm{Rb}}^{\max}$ and larger choices of κ/κ_T and d. These experiments in combination with the theory quantify just how badly the laser beam depolarization introduced by these unwanted reflections within the torpedo cell attenuates the maximum P_{Xe} achieveable at a given laser power. In all likelihood this is the explanation for the experimental practice of limiting the laser beam penetration in studies using torpedo cells of this type when high polarizations are desired.

A much larger $T_1^{\mathrm{Xe}*}$ was measured in the high quality optical container in comparison to the value found in the torpedo cell. This larger number is realistic as the temperature is 20 °C less which gives a smaller N_{Rb} and the volume is larger which minimizes collisions of the Xe with the container walls. The measured $m/b=0.3$ W in the high quality optical cell agrees much better with theory than that observed in the torpedo cell. A value of $m'/b'=0.3$ W can be obtained from Eq. (46) when a Gaussian beam radius of $d=2.4$ mm is used. This beam waist agrees with the value actually measured in the laboratory, $d=2.7$ mm, when the error present in both the laser power and beam chopping measurements are taken into account. No photon depolarization corrections were applied in this case since the high field optical spectra in this container indicate that there are just photons of the proper polarization present.[15] The incident laser power used in Fig. 6 is also scaled by 16% of its measured value. This is to account for the attenuation of the laser beam when passed through the sample off resonance of any optical transition (~32%). This loss in laser power arises from a reflection of the beam at the Pyrex windows on the sample container and the entrance to the NMR probe and sample oven (4 windows=8 interfaces). This reflection is due to the different indices of refraction of Pyrex and air. As a rule of thumb, uncoated Pyrex/air interfaces typically reduce laser powers by ~4%.

The comparison of experimental measurements of m'/b' to the values shown in Eqs. (32) and (46) provide an indirect measure of the Rb ground state electron T_1^{Rb} as m'/b' is extremely sensitive to ϵ. The theoretical value of ϵ can be calculated at for example $T=90$ °C from Eq. (17) for a Xe gas pressure ~1 atm using the published values of $\langle\sigma\overline{v}\rangle=2\times10^{-16}$ cm^3/s (Ref. 16) and $T_1^{\mathrm{Rb}}=20$ ms (Ref. 17) in combination with the measured value of $T_1^{\mathrm{Xe}*}=43$ min. This relaxation factor, $\epsilon=478$ s^{-1}, compares rather poorly with the value, $\epsilon=36\,616$ s^{-1}, that provides the best fit to the data in Figs. 5 and 6. There is some question on the usage of the T_1^{Rb} found in the literature in this type of calculation. The measurement was accomplished in a low magnetic field, $B_0=5$ G, i.e., not in the multi-tesla magnetic fields that we are operating in. Furthermore, that experiment measured the relaxation time of the $F=3\rightarrow F=2$ transition in the $^2S_{1/2}$ state in ^{85}Rb that has a 3.04 GHz level spacing. The relaxation rate actually needed for this calculation is likely to be quite different. Since the free electron spin flip transition is at 66 GHz in our case (see Figs. 1 and 2), it is easy to justify an order of magnitude difference in T_1^{Rb}. Even then, using a $T_1^{\mathrm{Rb}}\sim1$ ms gives $\epsilon=1428$ s^{-1} which still does not account for the much larger value, $\epsilon=36\,616$ s^{-1}, used to reconcile the data shown in Figs. 5 and 6.

This discrepancy lead us to measure T_1^{Rb} in high field using the Franzen technique.[18] These experiments will be reported on in more detail in a future publication.[19] In accord with the data reported here, the measured T_1^{Rb} in a variety of circumstances in magnetic fields of 2.35 T and 7.0 T is only on the order of tens of μs. This unexpectedly large effective electron relaxation rate at high fields in our samples is probably due to radiation trapping effects.[12] This becomes a dominant ground state spin relaxation mechanism during the optical pumping of Rb at large number densities. Including a value of $T_1^{\mathrm{Rb}}=28$ μs measured for the cell used here gives a more reasonable value of $\epsilon=36\,142$ s^{-1}.

Leakage relaxation of the Rb electron to ^{131}Xe also contributes to ϵ. It has been noticed both theoretically and experimentally[20] that $\langle\sigma\overline{v}\rangle$ for Rb–^{129}Xe is ~11.6 times larger than that for Rb–^{131}Xe. This factor of 11.6 comes from the square of the ratio of the ^{129}Xe/^{131}Xe gyromagnetic ratios. This alone would make $T_{1,Q}^{\mathrm{se}}\sim11.6T_1^{\mathrm{se}}=740$ min. This value in combination with the pressure dependent ^{131}Xe relaxation time[21] of $T_1^{XQ}=27$ s at 1 atm gives the ^{131}Xe contribution to the Rb leakage relaxation, $\alpha_Q\gamma_Q/T_1^{XQ}=474$ s^{-1}.

In certain samples N_2 buffer gas is included at 10% of the total sample pressure. Accounting for this leakage mechanism adds a factor of $\alpha_{\mathrm{N}}\gamma_{\mathrm{N}}/T_1^{\mathrm{N}}=7$ s^{-1}. A value for γ_{N} can be obtained from published measurements of the density dependent ^{14}N relaxation time in N_2 gas,[22] $T_1^{\mathrm{N}}\sim50$ μs, and the values for the Rb–^{129}Xe (Ref. 16) and Rb–N_2 (Ref. 23) spin exchange cross sections, $T_{1,N}^{\mathrm{se}}\sim(\sigma_{\mathrm{Xe}}/\sigma_{\mathrm{N}})T_1^{\mathrm{se}}=261T_1^{\mathrm{se}}=1307$ min. Combining all of the leakage relaxation factors together using Eq. (47) gives $\epsilon=36\,623$ s^{-1}. This is in much better agreement with the value used to model the data shown in Figs. 5 and 6. Clearly, the measurement of ^{131}Xe, Rb, and ^{14}N T_1's in our pumping cells at various temperatures and high field is necessary to more fully validate and to provide a complete accounting of the theory developed above. In any event however, these additional leakage factors can be seen to be quite small, and the portion of the current data presented herein is sufficient to ascertain that the theory presented represents the basic physics of the spin exchange pumping process.

VI. CONCLUSIONS

This study has shown that the optical pumping of nuclear spins in high fields can be quantitatively modeled using ideas from simple spin lattice relaxation theory. The results obtained indicate that more efficient optical pumping can be obtained by elimination of depolarized photons in the sample. There are in general three ways of accomplishing this. One introduced here uses the spectral dispersion of the Zeeman shifts in high magnetic fields to shift the pressure broadened atomic absorptions off resonance of any depolarized photons. An auxiliary to this approach is to decrease the Xe gas pressure used at any given field strength. As the number density of Xe is decreased the pressure broadening of the Rb atomic lines is reduced, and any depolarized pho-

tons will appear off resonance. These two approaches will work for any type of sample container. The third way of eliminating these effects is by optimizing the optical characteristics of the sample container to eliminate beam reflections and depolarization of the laser light. The latter is also important for low field pumping experiments. Adoption of these experimental practices can potentially enhance the laser power efficiency of commonly used optical pumping setups for producing spin polarized ^{129}Xe by over an order of magnitude. Such considerations have significant implications for the engineering of practical sources of polarized nobel gases in magnetic resonance imaging applications.[24]

In addition, high field operation provides better suppression of leakage relaxation of the ^{129}Xe. For these measurements, the leakage factor γ was found to be quite close to 1. Comparison to low field experiments shows that γ is often only the order of 0.5, thereby limiting the maximum achievable polarization. One must also pay careful attention to the composition of the pumping cell when very high polarizations are wanted. Leakage of the Rb polarization through cross relaxation to either ^{131}Xe or $^{14}N_2$ can have the potential for limiting the ultimate achievable ^{129}Xe polarization.

The most significant leakage mechanism identified in this work is due to the short effective T_1^{Rb} observed in high fields. Much longer T_1^{Rb} values have been observed at low Rb number densities in coated cells and with low buffer gas pressures at low fields. It is unknown at present whether much longer T_1^{Rb} values can be obtained at high fields with other combinations of sample composition or cell preparation. If this is possible, the greater efficiency afforded by optical pumping in high fields would make the production of large amounts of spin polarized ^{129}Xe feasible with the much smaller power levels produced by inexpensive laser diodes.

Minimizing the effects of photodepolarization produced in cases where the optical quality of the pumping containers is not insured, as well as supressing leakage relaxation by using enriched ^{129}Xe gas, are two ways of making the optical pumping of ^{129}Xe gas more efficient. To further maximize the polarization of ^{129}Xe gas one can take advantage of the geometry dependence of the volume averaged signal shown in Eq. (30). In the limit that the laser beam is much narrower than the sample, $r \gg d$, the maximum polarization is reduced to $2d^2/[r^2 \ln(2)]$. On the other hand when the laser intensity profile is flat over the sample, $r \ll d$, the maximum polarization is 1. This reduction due just to geometry considerations can be quite substantial. Consider the high quality optical cell discussed above where a laser beam waist of $d=2.4$ mm and a sample radius of $r=10.6$ mm was used. The maximum volume averaged polarization in this case is reduced from $P_{\mathrm{Rb}}^{\max}=1$ which was expected from the high field optical spectra in this container to $P_{\mathrm{Rb}} \sim 0.1$. Just by using a wider laser beam a 90% increase in pumping efficiency can be realized in this container since $P_{\mathrm{Rb}} \sim 1$ as $r \ll d$.

Using the theory outlined above in combination with some simple calculations the efficiency of a given pumping setup is easily determined. This permits one to optimize cell design and composition which is necessary when large reservoirs of nuclear spin polarized nobel gases are desired.

ACKNOWLEDGMENTS

Support of this work by the National Science Foundation under Grant No. CHE-9018455 is gratefully acknowledged. The authors would also like to acknowledge stimulating discussions with Patrick H. Vaccaro and Kurt Gibble for a critical reading of the manuscript.

[1] (a) A. Kastler, J. Phys. Radium **11**, 22 (1950); (b) J. Brossel, A. Kastler, and J. J. Winter, *ibid*. **13**, 668 (1952); (c) M. A. Bouchiat, T. R. Carver, and C. M. Varnum, Phys. Rev. Lett. **5**, 373 (1960); (d) R. M. Herman, Phys. Rev. A **137**, 1062 (1965); (e) W. Happer, Rev. Mod. Phys. **44**, 169 (1972); (f) B. C. Grover, Phys. Rev. Lett. **40**, 391 (1978).

[2] (a) D. Raftery, H. Long, T. Meersman, P. J. Grandinetti, L. Reven, and A. Pines, Phys. Rev. Lett. **66**, 584 (1991); (b) G. D. Cates, R. J. Fitzgerald, A. S. Barton, P. Bogorad, M. Gatzke, N. R. Newbury, and B. Saam, Phys. Rev. A **45**, 4631 (1992); (c) D. Raftery, H. Long, L. Reven, P. Tang, and A. Pines, Chem. Phys. Lett. **191**, 385 (1992); (d) M. Gatzke, G. D. Cates, B. Driehuys, D. Fox, W. Happer, and B. Saam, Phys. Rev. Lett. **70**, 690 (1993).

[3] (a) M. A. Bouchiat, T. R. Carver, and C. M. Varnum, Phys. Rev. Lett. **5**, 373 (1960); (b) R. M. Herman, Phys. Rev. A **137**, 1062 (1965); (c) W. Happer, Rev. Mod. Phys. **44**, 169 (1972); (d) B. C. Grover, Phys. Rev. Lett. **40**, 391 (1978).

[4] J. H. Noggle and R. E. Schirmer, *The Nuclear Overhauser Effect* (Academic, New York, 1971).

[5] M. Weissbluth, *Atoms and Molecules* (Academic, San Diego, 1978).

[6] A. A. Radzig and B. M. Smirnov, *Reference Data on Atoms, Molecules, and Ions*, Springer Series in Chemical Physics #31 (Springer, New York, 1985).

[7] (a) X. Zeng, Z. Wu, T. Call, E. Miron, D. Schreiber, and W. Happer, Phys. Rev. A **31**, 260 (1985); (b) W. Happer, T. Miron, S. Schaefer, D. Schreiber, W. A. van Winjingaarden, and X. Zeng, *ibid*. **29**, 3092 (1984); (c) G. D. Cates, R. J. Fitzgerald, A. S. Barton, P. Bogorad, M. Gatzke, N. R. Newbury, and B. Saam, *ibid*. **45**, 4631 (1992).

[8] (a) E. M. Purcell, H. C. Torrey, and R. V. Pound, Phys. Rev. **69**, 37 (1946); (b) N. Bloembergen, E. M. Purcell, and R. V. Pound, *ibid*. **73**, 679 (1948).

[9] A. Abragam and M. Goldman, *Nuclear Magnetism: Order and Disorder* (Oxford University, New York, 1982), p. 166.

[10] (a) H. Boersch, W. Raith, and M. Rehmet, Z. Phys. **163**, 197 (1961); (b) W. Raith, *ibid*. **163**, 467 (1961).

[11] R. C. Hilborn, Am. J. Phys. **50**, 982 (1982).

[12] (a) D. Tupa, L. W. Anderson, D. L. Huber, and J. E. Lawler, Phys. Rev. A **33**, 1045 (1986); (b) D. Tupa and L. W. Anderson, *ibid*. **36**, 2142 (1987).

[13] R. L. Streever and H. Y. Carr, Phys. Rev. **121**, 20 (1961).

[14] R. Freeman and H. Hill, J. Magn. Reson. **4**, 366 (1971).

[15] M. P. Augustine and K. W. Zilm, Mol. Phys. (in press).

[16] M. P. Augustine and K. W. Zilm, Chem. Phys. Lett. (in press).

[17] H. M. Gibbs and R. J. Hull, Phys. Rev. **153**, 132 (1967).

[18] W. Franzen, Phys. Rev. **138**, 850 (1959).

[19] M. P. Augustine and K. W. Zilm (in preparation).

[20] T. M. Kwon, J. G. Mark, and C. H. Volk, Phys. Rev. A **24**, 1894 (1981).

[21] F. J. Adrian, Phys. Rev. **138**, A403 (1965).

[22] C. J. Jameson, K. A. Jameson, and M. A. ter Horst, J. Chem. Phys. **95**, 5799 (1991).

[23] R. J. McNeal, J. Chem. Phys. **37**, 2726 (1962).

[24] M. S. Albert, G. D. Cates, B. Driehuys, W. Happer, B. Saam, C. S. Springer, and A. Wishnia, Nature **370**, 199 (1994).